



HAL
open science

A TEM study of a dislocations in the β_0 phase of an intermetallic TNM-TiAl alloy

Guy Molénat, Jean-Philippe Monchoux, Michael Musi, Petra Spoerk-Erdely, Helmut Clemens, Alain Couret

► **To cite this version:**

Guy Molénat, Jean-Philippe Monchoux, Michael Musi, Petra Spoerk-Erdely, Helmut Clemens, et al.. A TEM study of a dislocations in the β_0 phase of an intermetallic TNM-TiAl alloy. Scripta Materialia, 2022, 226, 10.1016/j.scriptamat.2022.115247 . hal-04283350

HAL Id: hal-04283350

<https://hal.science/hal-04283350v1>

Submitted on 15 Nov 2023

HAL is a multi-disciplinary open access archive for the deposit and dissemination of scientific research documents, whether they are published or not. The documents may come from teaching and research institutions in France or abroad, or from public or private research centers.

L'archive ouverte pluridisciplinaire **HAL**, est destinée au dépôt et à la diffusion de documents scientifiques de niveau recherche, publiés ou non, émanant des établissements d'enseignement et de recherche français ou étrangers, des laboratoires publics ou privés.

A TEM study of $a\langle 001 \rangle$ dislocations in the β_0 phase of an intermetallic TNM-TiAl alloy

Guy Molénat^(a), Jean-Philippe Monchoux^(a), Michael Musi^(b), Petra Spoerk-Erdely^(b), Helmut Clemens^(b), Alain Couret^(a)

^a CEMES, Université de Toulouse, CNRS, 29 rue Jeanne Marvig, BP 94347, 31055 Toulouse, France,

^b Department of Materials Science, Montanuniversität Leoben, Franz-Josef-Straße 18, 8700 Leoben, Austria

Abstract

The structure and mobility of $a\langle 001 \rangle$ dislocations in the β_0 phase of an intermetallic TNM-TiAl alloy produced by Spark Plasma Sintering were investigated by transmission electron microscopy. We find that these dislocations are dissociated into two identical superpartial dislocations separated by a stacking fault. Furthermore, $a\langle 001 \rangle$ dislocations are elongated along their screw orientation and are anchored to nano-sized precipitates of the ω_0 phase. *In situ* room temperature straining experiments show that dislocation propagation occurs through jumps between these elongated configurations.

Keywords: TNM TiAl alloy; Dislocations; Transmission electron microscopy; dissociation of dislocations; nano-sized precipitates

Despite the huge interest in β/β_0 -phase-containing TiAl alloys for applications in structural engineering, the structure and mobility of dislocations in the ordered β_0 phase have not been described in detail. Morris *et al.* [1,2] reported that in a Ti-44Al-2Mo (in at.%) alloy, two populations of dislocations can be activated in the β_0 phase, *viz.*, the $a\langle 001 \rangle$ dislocations and the $a\langle 111 \rangle$ superlattice dislocations. In our recent work [3] on a TNM alloy (Ti-43.5Al-4Nb-1Mo-0.1B (in at.%) [4,5]), prepared by Spark Plasma Sintering (SPS) [6], we established that the presence of mobile $a\langle 111 \rangle$ superlattice dislocations in the β_0 phase provides sufficient plasticity to avoid initiation of fracture of the specimen in this phase. It was also found that the mobility of these dislocations is hindered by fine nano-sized precipitates of the ω_0 phase, which incidentally, have been reported to be present in the β_0 phase of Nb-containing TiAl alloys (see [7,8] for some examples). The present paper reports a study of $a\langle 001 \rangle$ dislocations activated in the β_0 phase of the same as-SPSed TNM alloy [3] deformed at room temperature. In our study, we used two TEM (Transmission Electron Microscopy) techniques to explore the behaviour of these dislocations. First, we studied the deformation microstructure of thin foils extracted from bulk samples that were previously deformed (*ex situ*) in tension at room temperature. The second method consisted of *in situ* tensile tests inside a TEM to directly observe the dislocation dynamics under stress and in real time. More details on the experimental tools, as well as a description of the microstructure and mechanical properties of the TNM-Ti Al alloy used in this study can be found in our previous work [3].

Figs. 1 and 2 show representative $a\langle 001 \rangle$ dislocations of the β_0 phase of a TNM sample deformed at room temperature. The determination of the Burgers vectors and the characteristics of these dislocations were verified by studying several other similar dislocation microstructures not shown here. On micrographs taken with a (002) diffraction vector (Figs. 1(a) and 2(a)), the dislocations appear as paired. They are seen to be separated by fringes when using for example, the $(10\bar{1})$ diffraction vector (Fig. 1(b)). When using the $(\bar{1}10)$ and (110) diffraction vectors,

both the dislocations of a pair are out of contrast in Figs. 2(b) and (c). Hence, the Burgers vector \mathbf{b} of these dislocations has to be parallel to the [001] direction. Consistently, these dislocations have been observed to be out of contrast with (200) or (020) diffraction vectors perpendicular to the Burgers vector direction (situations not reproduced here). Furthermore, the similarity in contrast of the two dislocations of a given pair (Figs. 1 (a) and 2(a)) indicates that they have the same Burgers vector.

The presence of a fringe contrast (Fig. 1(b)) implies that a stacking fault (SF) or an antiphase boundary (APB) separates the two dislocations of a pair. The set of micrographs in Figs. 2 (d, e, f) complements Fig. 2 (a); Fig. 2 (d) depicts the contrast obtained with the fundamental diffraction vector of the opposite sign ($00\bar{2}$), while Figs. 2 (e) and (f) show micrographs obtained with the two superlattice reflections (001) and ($00\bar{1}$), respectively. Since superlattice reflections do not show fringe contrast, we infer that the fault separating the two paired dislocations is a stacking fault rather than an antiphase boundary. On the other hand, we note that a fringe contrast is detected with the ($10\bar{1}$) diffraction vector, which is not perpendicular to the Burgers vector direction (Fig. 1 (b)), but this contrast disappears with both the ($\bar{1}10$) and (110) diffraction vectors, which are perpendicular to \mathbf{b} (Figs. 2 (b) and (c), respectively). This fringe contrast can be fully explained using the classical stacking fault extinction criterion ($\alpha = 2\pi\mathbf{g}\cdot\mathbf{R} = 0$, with $\mathbf{R}=\mathbf{b}$ in this case), which is not satisfied in the case shown in Fig. 1 (b). Furthermore, tilt experiments (not reproduced here) have shown that the stacking fault may be spread in {200} and {110} planes, which are in zone around the direction of the Burgers vector. Taken together, this whole set of elements is consistent with the following dissociation scheme of the $a[001]$ Burgers vector: $a[001] \rightarrow a/2 [001] + \text{SF} + a/2 [001]$. We point out here that this type of dislocation is observed in deformed samples as well as in thin foils extracted from undeformed samples. In the latter case, we believe that the deformation microstructure could stem either from the sample preparation procedure or be created during the preparation of the

alloy, where thermal stress could be generated during cooling from high temperature. Consequently, it is difficult to affirm that these dislocations are formed only during the tensile tests.

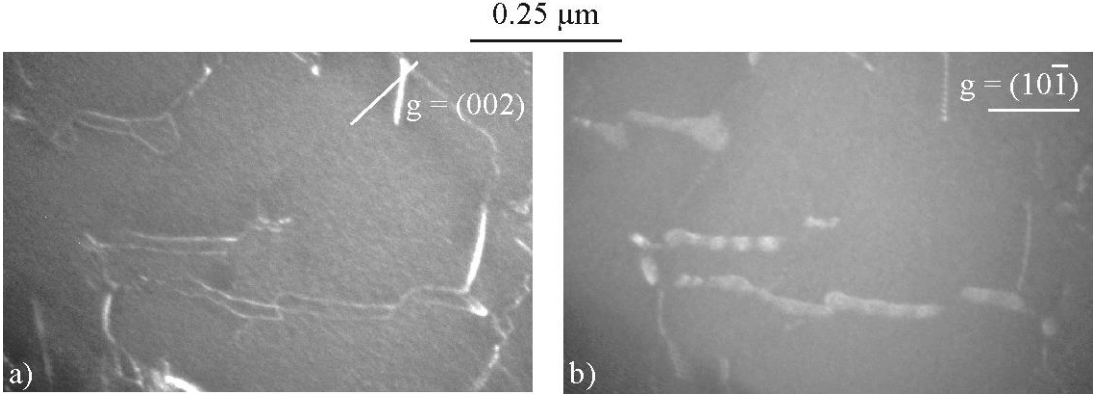


Fig. 1. TEM images of the same $a[001]$ dislocations under two diffraction conditions (see text).

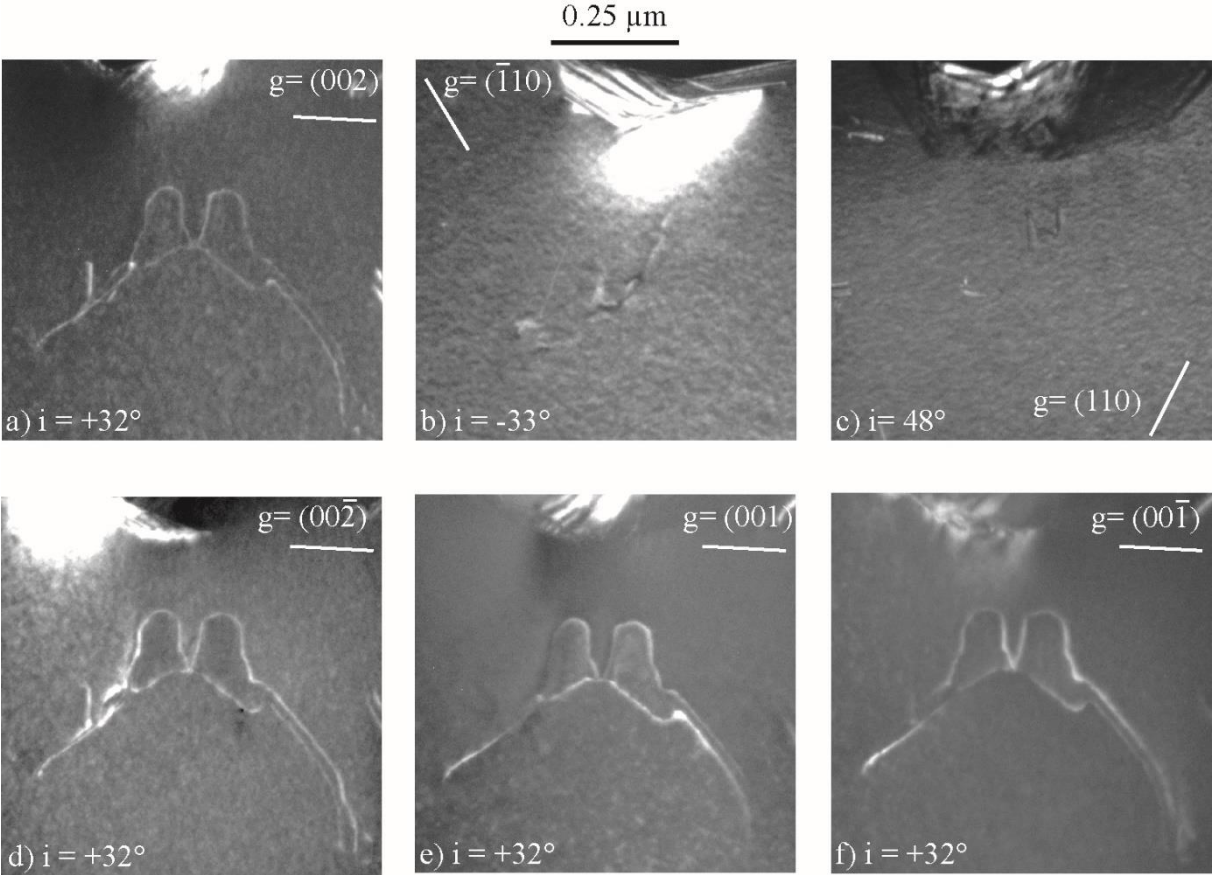


Fig. 2. TEM images of the same $a[001]$ dislocation under six diffraction conditions (see text).

Fig. 3 (a) shows three pile-ups (marked PU1, PU2 and PU3) in a thin foil extracted from a specimen deformed at room temperature. Figs. 3 (b)–(e) focus on the tip of PU1 with four other diffraction vectors, and Tab. 1 summarizes the contrast characteristics for the five diffraction conditions. Contrast analysis reveals that pile-up PU1 contains two types of dislocations: $a[010]$ dislocations that are out-of-contrast in Fig. 3 (c), and $a[111]$ superlattice dislocations which are out-of-contrast in Fig. 3 (d). In Fig. 3 (b), both types are in contrast, as in Fig. 3 (a). The Burgers vector \mathbf{b} of dislocations marked D1 and D5 is $a[111]$, and \mathbf{b} of D2, D3, D4 and D6 is $a[010]$. Stereographic analysis and tilt experiments (not reproduced here) demonstrated that the pile-up lies in the $(\bar{1}01)$ plane, which contains these two Burgers vectors. Because the $(\bar{1}01)$ glide plane is unambiguously known in this case, the Schmid factors for both deformation systems can be calculated and these values are nearly identical, i.e., 0.37 ± 0.05 for $a[010]$ dislocations and 0.38 ± 0.05 for $a[111]$ dislocations. For dislocation D3, Figs. 3 (e) and (b) allow to discern certain features: i) Fig. 3 (e) taken with a diffracting vector parallel to the $a[010]$ Burgers vector allows to detect local separations of the two partial dislocations $a/2[010]$ (marked by two yellow arrows). ii) In Fig. 3 (b) where the diffracting vector (110) is not perpendicular to the $[010]$ direction, a fringe contrast between these two partial dislocations can be detected (circled in dashed yellow line). Therefore, we deduce that $a[010]$ dislocations are dissociated following the same dissociation scheme as the dislocations observed in Figs. 1 and 2, but with a shorter separation distance between the two partial dislocations. In the other pile-ups (PU2 and PU3), no $a[111]$ superlattice dislocations were observed and dissociation into partial dislocations was not detected. Figs. 3 (a) and (d) show that the $[010]$ dislocations are anchored at small pinning points. The concentration of dislocations in pile-ups and the presence of $a[111]$ superlattice dislocations in one of them lead us to believe that the dislocation microstructure was indeed

created during the tensile deformation of the sample. Moreover, the high Schmid factor values for both deformation systems support this claim.

Tab. 1. Contrast characteristics for the two dislocation families, $a[111]$ and $a[010]$, for five different diffraction vectors used in Figs. 3 (a-e).

Image	g-vector	b=$a[111]$	b=$a[010]$
Fig. 3 (a)	$(0\bar{1}1)$	In contrast	In contrast
Fig. 3 (b)	(110)	In contrast	In contrast
Fig. 3 (c)	(101)	In contrast	Out of contrast
Fig. 3 (d)	$(\bar{1}10)$	Out of contrast	In contrast
Fig. 3 (e)	(010)	In contrast	In contrast

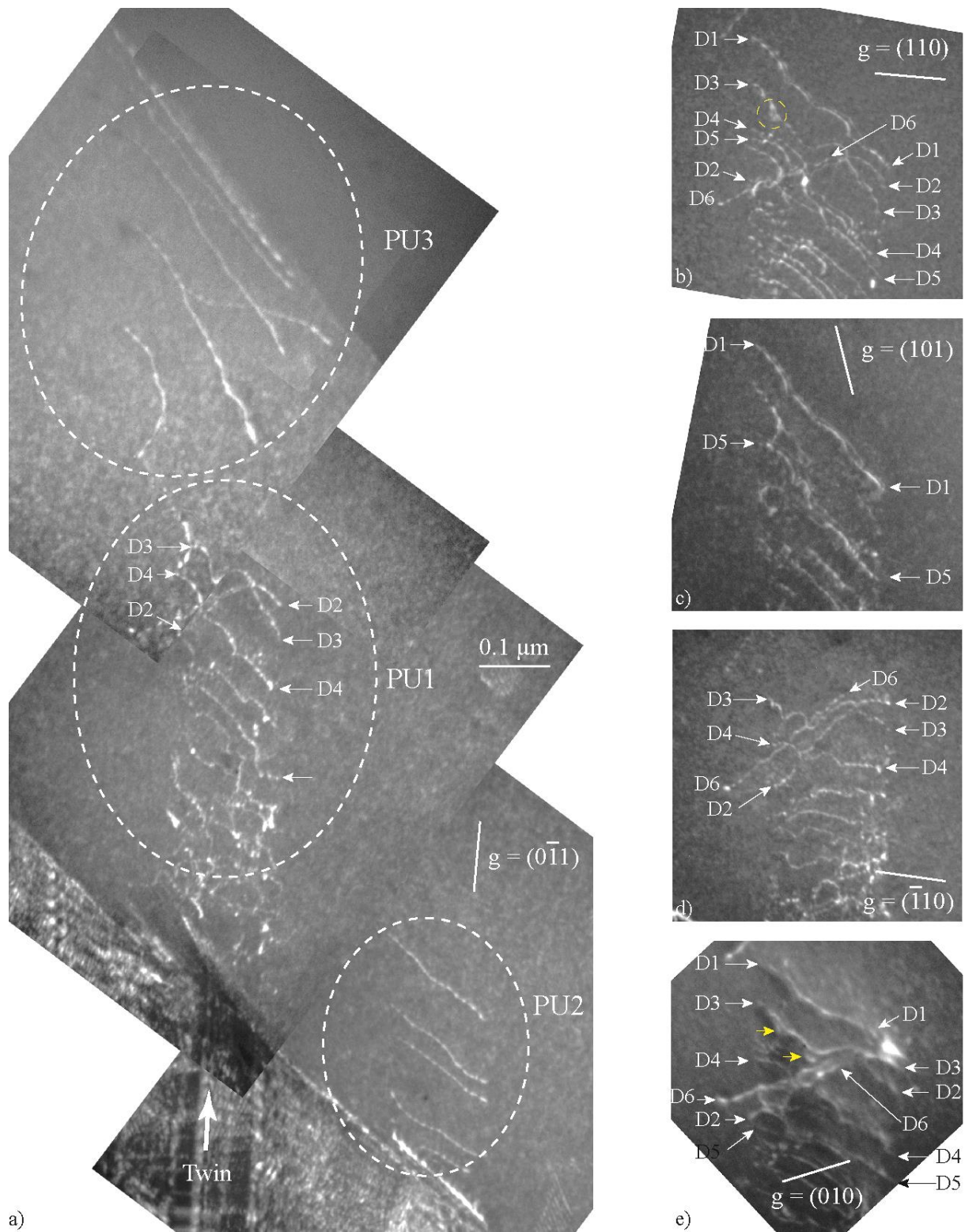


Fig. 3. Three pile-ups of dislocations (PU1, PU2 and PU3) as observed by TEM. The tip of the pile-up PU1 is monitored under different diffraction conditions as shown in micrographs (b) to (e).

Fig. 4 shows the movement of $a\langle 001 \rangle$ dislocations under stress during an *in-situ* straining experiment. We note here that the dislocations show no apparent dissociation under the imaging conditions used. This figure is a montage made from images extracted from the video available [here](#). This video, which is in real time, was extracted from a longer one. In Fig. 4, the different images taken from the video have been rotated 20° counter clockwise so that the average elongation direction of the dislocations is in the vertical direction. The dislocations move from left to right. Using the $\mathbf{g}\cdot\mathbf{b} = 0$ criterion, the Burgers vector of these dislocations was determined to be $a[100]$. The projection of this direction in the image plane b_p is shown in Fig. 4(b), which indicates that on average, the dislocations are extended along their screw direction. Stereographic analysis based on electron diffraction patterns show that the slip traces left by moving dislocations on the thin foil surfaces (marked by black triangles in Fig. 4(h)) are parallel to the (011) plane, which is a glide plane for these dislocations. Figs. 4(b) to (d) display the overall movement of a D4 dislocation, whose successive positions are marked by yellow triangles on each micrograph (during this sequence, dislocations D2 and D3 stay in place and D1 moves forward as detailed below). Each D4 jump takes less than a $1/25$ s, which is the period between two consecutive video frames. Figs. 4(e)–(i) display the different elementary steps during the movement of dislocation D1. The dislocation's motion results from a succession of forward jumps of short screw segments and lateral propagations of non-screw segments. Each arrow indicates an elementary movement. For example, between Figs. 4(e) to (f), a short screw segment has moved and adopted on a curved shape. Between Figs. 4(f) to (g), the arrowed segments have also moved forward. Between Figs. 4(g) and (h), the dislocation escaped from the encircled pinning points, causing the previously anchored segments to glide, as indicated by the arrows. The upward movement is due to the dislocation escaping from the pinning, whereas the downward movement is due to the anchored non-screw segments propagating laterally. Between Figs. 4(h) and (i), the dislocation once again escaped the

constraint of a pinning point. Similar to the jumps of dislocation D4, all of these elementary movements happen in less than 1/25 s. As reported previously for ordinary dislocations in γ -TiAl based alloys [9], the escaping of the dislocation from pinning points is most likely caused by movements of anchored segments until a critical configuration is reached that allows the dislocation to escape. The projected distance between the pinning points was estimated to be about 35 nm, which corresponds to an actual distance of 45 nm, considering the tilt of the gliding plane with respect to the picture plane.

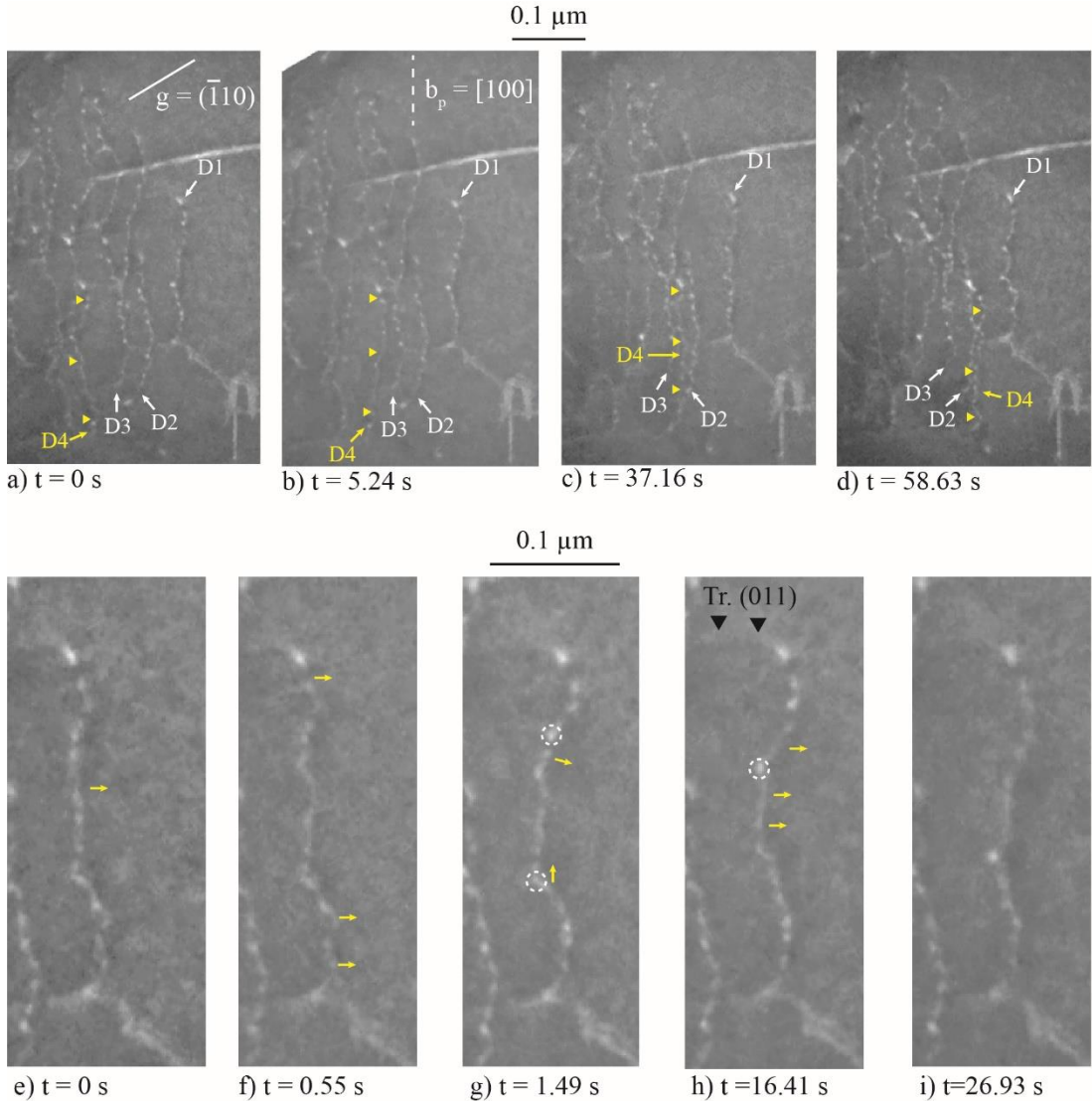


Fig. 4. Images extracted from a video showing the movement of a[100] dislocations observed during a tensile test performed inside the TEM. (a)–(d): movement of dislocation D4. (e)–(i) elementary steps in the movement of dislocation D1. All the movements described in the text are indicated in yellow arrows and lettering.

The current TEM work has shown that $a\langle 001 \rangle$ dislocations are activated in the β_0 phase of a TNM alloy in addition to the previously observed $a\langle 111 \rangle$ superlattice dislocations [3], which is in agreement with the study of Morris *et al.* [1,2] conducted on Ti-44Al-2Mo (in at.%) alloy. More generally, these two types of dislocations have been observed in other intermetallic alloys with the B2 structure. For example, FeAl and NiAl intermetallic aluminides show different behaviour since the former is deformed only by $a\langle 111 \rangle$ dislocations [10,11] and the latter by both $a\langle 001 \rangle$ and $a\langle 111 \rangle$ dislocations [12]. The activation of $a\langle 111 \rangle$ dislocations in addition to $a\langle 001 \rangle$ has been explained based on the tendency of $a\langle 111 \rangle$ superdislocations to dissociate. Indeed, since the Burgers vector of $a/2\langle 111 \rangle$ superpartials is shorter than that of $a\langle 001 \rangle$ dislocations [13], the dissociation process promotes the motion of the former. Using atomistic calculations, it has been shown that the determination of the active deformation process is linked to an interplay between the mobility of dislocations resulting from their core structure, their energy, and the energy of possible planar faults [14]. In the pile-up PU1, both families of dislocations ($a\langle 111 \rangle$ and $a\langle 001 \rangle$) are observed (Fig. 3). As seen at the bottom of Fig. 3(a), this pile-up could have resulted from the interaction of incident twins with a grain boundary, most likely through a deformation transmission process as often observed at lamellar interfaces and grain boundaries of γ -TiAl based alloys [15,16]. The activation of these two dislocation families under identical Schmid factors suggests that they are mobile under equivalent critical resolved shear stresses, which is consistent with their coexistence in the ordered β_0 phase.

The presence of identical $a\langle 001 \rangle$ dislocations in bulk deformed samples (Fig. 3) and in *in situ* experiments (Fig. 4), as well as the simultaneous activation of both $a\langle 001 \rangle$ and $a\langle 111 \rangle$ dislocations in the same pile up (Fig. 3), allows to conclude that $a\langle 001 \rangle$ dislocations are mobilized during plastic deformation of the β_0 phase. These dislocations show very little dissociation, if any (Figs. 3(b) and (e)). The origin of the much wider dissociated $a\langle 001 \rangle$ dislocations, as observed in bulk samples (Figs. 1 and 2), remains an open question. It is

tempting to speculate that widely dissociated $a\langle 001 \rangle$ dislocations are formed at high temperatures during the SPS cycle, prior to the precipitation of ω_0 , which is known to occur during subsequent cooling to room temperature [17]. Nonetheless, the detailed examination of these widely dissociated dislocations based on Fig. 1 and 2 allowed to extend our understanding on the general structure of $a\langle 001 \rangle$ dislocations.

We have shown that the dissociation of $a\langle 001 \rangle$ dislocations corresponds to two identical partial dislocations bordering a stacking fault, according to the scheme: $a\langle 001 \rangle \rightarrow a/2\langle 001 \rangle + \text{SF} + a/2\langle 001 \rangle$. This dissociation scheme is unexpected, since previously reported literature rather suggests a splitting into two non-identical partial dislocations of the type $a/2\langle 111 \rangle$ [14], a dissociation scheme that is clearly incompatible with our TEM observations. Nevertheless, extended fault contrasts associated with $a\langle 001 \rangle$ dislocations have been previously observed by Viguier et al. [18] in a B-containing FeAl alloy with a dislocation scheme that corresponds at first approximation, to that proposed in this work, with two identical $a/2\langle 001 \rangle$ partial dislocations bordering a fault. However, these authors observed fringe contrasts when using $\{110\}$ diffraction vectors perpendicular to the fault displacement vector, which were not detected in the present work under the same contrast conditions of. This fringe contrast, which could not be explained by residual contrast or a simple planar fault, was interpreted by Viguier et al. [18] to be due to the presence of a small out-of-plane fault component arising from the segregation of the B atoms (substituting for Al atoms) on the (100) plane, according to the following dissociation scheme: $a\langle 001 \rangle \rightarrow a\langle 0\delta 1/2 \rangle + a\langle 0\bar{\delta} 1/2 \rangle$, where δ reflects the limited out-of-plane component.

Similar to the $a\langle 111 \rangle$ superlattice dislocations analysed elsewhere [3], $a\langle 001 \rangle$ dislocations, when observed in motion during *in situ* straining tests, are clearly seen to be anchored at small pinning points. Because the measured average distances between the pinning points anchoring both $a\langle 001 \rangle$ dislocations and $a\langle 111 \rangle$ superlattice dislocations are close (45 nm here for

$a\langle 001 \rangle$, 35 nm for $a\langle 111 \rangle$ in [3]), it appears likely that anchoring of $a\langle 001 \rangle$ dislocation also occurs on ω_0 precipitates. A more detailed investigation of this nano-precipitation process by combining several electron microscopy techniques such as conventional imaging, lattice imaging, and *in situ* experiments, is underway.

Several characteristics of $a\langle 001 \rangle$ dislocations' mobility can thus be highlighted. Firstly, they are less concentrated in pile-ups than $a\langle 111 \rangle$ superlattice dislocations, and decorrelated partial dislocation motions are not observed. Secondly, the dissociation width appears to be quite limited, at least for those cases where we are sure that the dislocations were moving under stress (Figs. 3 and 4). Thirdly, $a\langle 001 \rangle$ dislocations move by a combination of forward screw segment jumps and lateral propagations of anchored non-screw segments, in combination with larger but limited jumps of the whole dislocation. These three characteristics indicate that the behaviour of $a\langle 001 \rangle$ dislocations is similar to that of ordinary dislocations in the γ phase of TiAl based alloys. In both cases, gliding of the dislocation is controlled predominantly by a frictional force due to a slight dislocation core spreading, with anchoring on extrinsic chemical pinning points playing only a secondary role [9].

In conclusion, our TEM analysis reveals that, in addition to the $a\langle 111 \rangle$ superlattice dislocations, $a\langle 001 \rangle$ dislocations contribute to the deformation of the β_0 phase of a TNM alloy containing nano-sized ω_0 precipitates. These dislocations are weakly dissociated into two identical partial dislocations and anchored to these precipitates.

Acknowledgements

This study has been conducted in the framework of the cooperative Austrian-French project “Hi-TiAl - 18-CE91-0008-01” jointly supported by the French Agence Nationale de la Recherche (ANR) and the Fonds zur Förderung der wissenschaftlichen Forschung (FWF). M.

Musi is a Recipient of a DOC Fellowship of the Austrian Academy of Sciences at the Department of Materials Science, Montanuniversität Leoben.

References

- [1] M.A. Morris, Y.G. Li, Deformation mechanisms and slip transfer in a Ti-44Al-2Mo alloy, *Materials Science and Engineering A* 197 (1995) 133-145.
- [2] M.A. Morris, Y.G. Li, Deformation mechanisms within the B₂, L1₀ and DO₁₉ structures of a Ti-44Al-2Mo alloy, *Gamma Titanium Aluminides*, Edited by Y.W. Kim, R. Wagner and M. Yamaguchi, The Mineral, Metals and Materials Society, (1995), 353-361.
- [3] G. Molénat, B. Galy, M. Musi, L. Toualbi, M. Thomas, H. Clemens, J.P. Monchoux, A. Couret, Plasticity and brittleness of the ordered β_0 phase in a TNM-TiAl alloy, *Intermetallics*, 151 (2022) 1-11
<https://doi.org/10.1016/j.intermet.2022.107653>.
- [4] H. Clemens, Wallgram W, Kremmer S, Güther V, Otto A, Bartels A, Design of Novel β -Solidifying TiAl Alloys with Adjustable β /B2-Phase Fraction and Excellent Hot-Workability, *Adv. Eng. Mater.* 10 (2008) 707.
- [5] S. Mayer, P. Erdelyi, F.D. Fischer, D. Holec, M. Kasthuber, T. Klein, H. Clemens, Intermetallic β -solidifying γ -TiAl based alloys: from fundamental research to application, *Adv. Eng. Mater.* 19-4 (2017) 1–27.
- [6] A. Couret, T. Voisin, M. Thomas, J.P. Monchoux, Development of a TiAl Alloy by Spark Plasma Sintering, *The Minerals, Metals & Materials Society*, 69-12 (2017) 2576-2582
<https://doi.org/10.1007/s11837-017-2549-6>
- [7] M. Schloffer, B. Rashkova, T. Schöber, E. Schwaighofer, Z. Zhang, H. Clemens, S. Mayer, Evolution of the ω_0 phase in a β -stabilized multi-phase TiAl alloy and its effect on hardness, *Acta Metall. Mater.*, 64 (2014) 241-252.
- [8] X. Wang, J. Yang, K. Zhang, R. Hu, L. Song, H. Fu, Atomic-scale observations of B2 \rightarrow ω -related phases transition in high-Nb containing TiAl alloy, *Materials Characterization*, 130 (2017) 135-138.
- [9] A. Couret, An in situ study of ordinary dislocations glide in TiAl alloys, *Phil. Mag. A*, 79 (1999) 1977-1994.
- [10] P. Veysseyre, R. Noebe, Weak-beam study of $\langle 111 \rangle$ superlattice, *Philosophical Magazine A*, 65 (1992) 1-13.
- [11] J.X. Yan, Z.J. Zhang, K.Q. Lia, Z.Y. Xia, J.B. Yang, Z.F. Zhang, Core structures and planar faults associated with $\langle 111 \rangle$ screw superdislocations in B2 alloys, *Intermetallics* 110 (2019) 1-7.
- [12] K. Benhaddan, P. Beauchamp, Core Structure of the $a\langle 100 \rangle \langle 001 \rangle$ Edge Dislocation in a B2 Ordered Alloy, *Phys. Stat. Sol. (a)* 98, (1986) 195-202.
- [13] Y. Q. Sun, Characteristics of $\langle 111 \rangle$ slip in a NiAl [001] single crystal, *Philosophical Magazine A*, 80 (2000) 447-465.
- [14] B.L. Lü, G.Q. Chen, S. Quc, H. Su, W.L. Zhou, Effect of alloying elements on $\langle 111 \rangle$ dislocation in NiAl: A first-principles study, *Physica B* 417 (2013) 9–12.
- [15] Zghal S., Couret A, Transmission of the deformation through gamma-gamma interfaces in a polysynthetically twinned TiAl alloy - II. Twin interfaces (180 degrees rotational), *Phil. Mag. A*, 81 (2001) 365-382.
- [16] J.P. Monchoux, J. Luo, T. Voisin, A. Couret, Deformation modes and size effect in near- γ TiAl alloys, *Materials Science & Engineering, A* 679 (2017) 123–132.

- [17] T. Voisin, L. Durand, N. Karnatak, S. Le Gallet, M. Thomas, Y. Le Berre, J.F. Castagne, A. Couret A, Temperature control during Spark Plasma Sintering and application to up-scaling and complex shaping, *Journal of Materials Processing Technology*, 213 (2013) 269-278.
- [18] B. Viguier, M. Martinez, J. Lacaze, Characterization of complex planar faults in FeAl(B) alloys, *Intermetallics* 83 (2017) 64-69.